Journal of Hazardous Materials 213–214 (2012) 299–310

Contents lists available at SciVerse ScienceDirect

Journal of Hazardous Materials

journal homepage: www.elsevier.com/locate/jhazmat

Removal of trichloroethylene DNAPL trapped in porous media using nanoscale zerovalent iron and bimetallic nanoparticles: Direct observation and quantification

Qiliang Wang[a,1], Seung-Woo Jeong[b,**], Heechul Choi[a,*]

[a] School of Environmental Science and Engineering, Gwangju Institute of Science and Technology (GIST), 261 Cheomdan-gwagiro, Buk-gu, 500-712 Gwangju, Republic of Korea
[b] Department of Environmental Engineering, Kunsan National University, Kunsan 550-701, Republic of Korea

ARTICLE INFO

Article history:
Received 1 August 2011
Received in revised form 30 January 2012
Accepted 1 February 2012
Available online 8 February 2012

Keywords:
TCE DNAPL
Glass micromodel
Porous media
NZVI
Bimetallic nanoparticles

ABSTRACT

Direct trichloroethylene (TCE) dense non-aqueous phase liquid (DNAPL) removal inside pore areas using nanoscale zerovalent iron (NZVI) and bimetallic nanoparticles were first investigated in a water-saturated porous glass micromodel. Effects of nitrate, aqueous ethanol co-solvent, humic substance, and elapsed time on TCE DNAPL removal using NZVI were studied by direct visualization. The removal efficiency was then quantified by directly measuring the remaining TCE DNAPL blobs area using an image analyzer. As ethanol content of co-solvent increased, TCE DNAPL removal by NZVI was also increased implying sequential TCE DNAPL removal mechanisms: as dissolved TCE was degraded by NZVI, TCE dissolution from TCE blobs would be then facilitated and the TCE blob areas would be eventually reduced. The presence of nitrate and humic substance hindered the NZVI reactivity for the TCE DNAPL removal. In contrast, the TCE DNAPL removal efficiency was enhanced using bimetallic nanoparticles in a short-term reaction by generating atomic hydrogen for catalytic hydro-dechlorination. However, all TCE DNAPL removal efficiencies reached the same level after long-term reaction using both NZVI and bimetallic nanoparticles. Direct TCE DNAPL observation clearly implied that TCE blobs existed for long time even though all TCE blobs were fully exposed to NZVI and bimetallic nanoparticles.

1. Introduction

Trichloroethylene (TCE), a representative dense non-aqueous phase liquid (DNAPL), is a ubiquitous contaminant in groundwater systems and has been the focus of considerable attention over the last 20 years [1–3]. Two distinct characteristics of TCE are its low water solubility and high toxicity. Additionally, TCE migrates downward until the less permeability strata of the subsurface is encountered, resulting in local saturations ranging from 1% to 70–80% [4]. Discontinuous immobile TCE blobs and pools can be continuous sources for groundwater contamination. The removal of TCE DNAPL from porous media is a difficult issue due to the heterogeneity of natural porous media systems, mass transfer limitations [5,6], and TCE dissolution instabilities [1,7]. Therefore, many technologies for detecting TCE removal efficiencies dominantly rely on the mass transfer from the TCE DNAPL to a mobile fluid phase [8,9].

Remediation strategies traditionally involve pumping contaminated groundwater to the surface and passing it through a treatment system, which either degrades the chlorinated compounds as in the case of advanced oxidation processes, or transfers to the other media as in the case of air stripping and the use of carbonaceous materials [10]. However, the difficulty in remediating contaminated aquifers with standard pumping methods is due in part to the slow dissolution rates of residual and pooled TCE DNAPL into water [11]. To overcome this problem, advanced and in situ technologies have been proposed: hydrophilic alcohol and surfactant solutions were used to enhance dissolution of entrapped TCE [12,13]. Zero valent iron (ZVI) dehalogenating TCE also employed anionic and nonionic surfactants for enhancement of TCE dissolution [14].

Recently, nanoscale zero-valent iron (NZVI) and bimetallic (Fe/Pd and Fe/Ni) nanoparticles have been used for in situ TCE dechlorination [3], based on the increased reactivity of nanoparticles due to their high surface area to volume ratio. NZVI can be modified using a surfactant more mobile to transport into water-saturated porous media for in situ application [15]. Compared to iron filings, bimetallic nanoparticles have much higher

* Corresponding author. Tel.: +82 62 715 2441; fax: +82 62 715 2434.
** Corresponding author. Tel.: +82 62 469 4767; fax: +82 62 469 4964.
E-mail addresses: swjeong@kunsan.ac.kr (S.-W. Jeong), hcchoi@gist.ac.kr (H. Choi).
[1] Present address: Department of Environmental Engineering and Earth Science, Clemson University, Clemson, United States.

0304-3894/$ – see front matter © 2012 Elsevier B.V. All rights reserved.
doi:10.1016/j.jhazmat.2012.02.002

TCE dechlorination rates and provide saturated hydrocarbon products [16]. In recent decades, several influencing factors, e.g., natural organic matter (NOM) and dissolvable mineral solute, on the reactivity and lifetime of NZVI in natural groundwater systems have been studied for degradation of aqueous phase dissolved TCE [17]. These factors have also been proved to be able to influence the aqueous dissolved TCE removal [18]; however, the effects of these factors on the performance of direct TCE DNAPL removal using NZVI in porous media have not yet been comprehensively studied.

Only few NZVI studies have been dealt with DNAPL not dissolved compounds: Berge and Ramsburg used a dense concentration of TCE dissolved in cosolvent (230 g/L) for their NZVI batch study [19]; Taghavy et al. evaluated NZVI for treatment of a PCE-DNAPL trapped in the column [20]; Phenrat et al. used dodecane-LNAPL for their study on the transport and contact of polymer-modified NZVI particles to the LNAPL source in 2-D sand box [21]. To the best of our knowledge, the fate and performance of NZVI and bimetallic nanoparticles for TCE DNAPL removal inside pore areas have never been directly visualized and quantified in porous media. To better observe the reaction between iron based nanoparticles and TCE DNAPL, and to more accurately quantify the TCE DNAPL removal using nanoparticles in an aquifer simulated system, an artificial transparent two-dimensional porous medium (i.e., a glass micromodel) can be a good research tool [22–25]. In addition, visualization of the TCE DNAPL removal using NZVI and bimetallic nanoparticles under a microscope can elucidate the removal mechanisms to explain "black box" phenomenon limitation of the soil column study. Therefore, the goal of this study is to directly visualize and quantify TCE DNAPL removal and mobilization of metallic nanoparticles in porous media using a glass micromodel under different influence factor conditions. To achieve this goal, our study will meet two objectives: (1) to understand the fate and transport of NZVI in the TCE DNAPL emplaced glass micromodel using a visualization technology; and (2) to investigate the effects of hydrophilic alcohol, nitrate, humic substance, and the catalytic properties of novel metals on the TCE DNAPL removal performance in a glass micromodel. Eventually, this study tried to find some implications of NZVI for groundwater remediation.

2. Experimental

2.1. Materials and methods

The chemicals used in this study (TCE, oil-red-o, $NaBH_4$, $NaHCO_3$, KCl, and $NaNO_3$) were reagent grade (obtained from Sigma–Aldrich, USA), and were used directly, as received, without pretreatment unless otherwise specified. In addition, $FeCl_3{\cdot}6H_2O$ and $CaCl_2{\cdot}2H_2O$ were obtained from Junsei (Japan), $MgCl_2{\cdot}6H_2O$ was purchased from Oriental Chemical Industries (South Korea), and ethanol (99.5%) was purchased from Duksan Chem. (South Korea). The electrolyte stock solutions were prepared and then filtered through 0.45 μm filters (Advantec MFS, Inc.) before use. Note that the NZVI and bimetallic nanoparticles were synthesized as described in the previous reports [16,17]. Experiments and measurements were conducted in synthetic groundwater (SGW), prepared close to Dries et al. [26]: $NaHCO_3$, KCl, $CaCl_2$, and $MgCl_2$ (0.5 mM each), with pH at 7.0 ± 0.1, and SGW purged using nitrogen to reduce the dissolved oxygen. Additionally, the model for naturally occurring soil humic substance, Pahokee peat fulvic acid (PPFA, 2S103F standard II), was purchased from the International Humic Substances Society (IHSS). All chemical stock solutions were prepared using doubly deionized water (18 MΩ Milli-Q) and stored at 4 °C prior to use.

Table 1
Physical properties of the glass micromodel.

Parameter	Value
2-D porous medium/(glass heterogeneous micromodel)	
Length, L	128 mm
Width, W	84 mm
Total porosity, ε	0.455
Pore volume, V_p	0.94 mL
Temperature	25 ± 2 °C
Flow rate of particles	10 mL/h
Flow rate of fluid	10 mL/h
approach	

2.2. Characterization of synthesized NZVI and bimetallic nanoparticles

X-ray diffraction (XRD) analyses were conducted in ambient air with Cu Kα using a Rigaku RINT 2000 wide-angle goniometer operated at 40 kV and 40 mA; continuous scans from 5° to 80° 2θ were performed with a step size of 0.01° and a count time of 5 s per step. Morphological analyses of the samples were performed by field emission scanning electron microscopy (FE-SEM) using a Hitachi 4700 microscope (at 15 kV) with energy-dispersive X-ray (EDX) analyses and high-resolution transmission electron microscopy (TEM) performed using a JEOL TEM 2100 FXII operated at 200 kV. X-ray photoelectric spectroscopy (XPS; Multilab 2000, Thermo Electron Corporation, England) was used for the analysis of iron nanoparticles to determine their surface composition to a depth of less than 5 nm. Hydrochloric acid (HCl) digestion was performed by dissolving NZVI and bimetallic nanoparticles into an HCl solution and measuring the H_2 (g) generated [27]; the component % of iron, nickel, and palladium in the original particles were determined using inductively coupled plasma mass spectrometry (ICP-OES; PerkinElmer, Optima 5300DV) after the nanoparticles were digested in HCl.

2.3. Preparation of co-solvent solution, SGW with PPFA, and nitrate solution

The aqueous ethanol co-solvent solution was prepared by diluting ethanol (99.5%) into 20% and 50% using DI water. SGW with PPFA as background solution was prepared by diluting the prepared PPFA stock solution into SGW at a pH of 7.0 ± 0.1. PPFA concentrations of 5, 10, and 15 ppm in the prepared target solutions were confirmed using total organic carbon (TOC) analysis based on the carbon content reported by the IHSS. Finally, $NaNO_3$ solution was prepared by diluting the stock solution to 40, 20, 10, and 4 mM using DI water.

2.4. Micromodel configuration, properties, and experimental setup

A two-dimensional porous medium made of etched glass was used in this study (Fig. 1a). The transparent porous medium is an artificial network model of interconnecting pores and throats. The irregular network pattern has a local microscopic heterogeneity due to variation in the grain shape and size. The utilization allows for the observation of bulk transport properties within the entire porous medium as well as the examination of microscopic mechanisms at a pore level. Table 1 shows the physical properties of the glass micromodel.

A schematic of the experimental apparatus is shown in Fig. 1b. A micromodel saturated with background solution was horizontally mounted on the light stage of a stereoscope (Motic SMZ 168) equipped with a Moticam 2500 CCD video camera that was mounted directly on its eyepiece. The experimental setup allowed

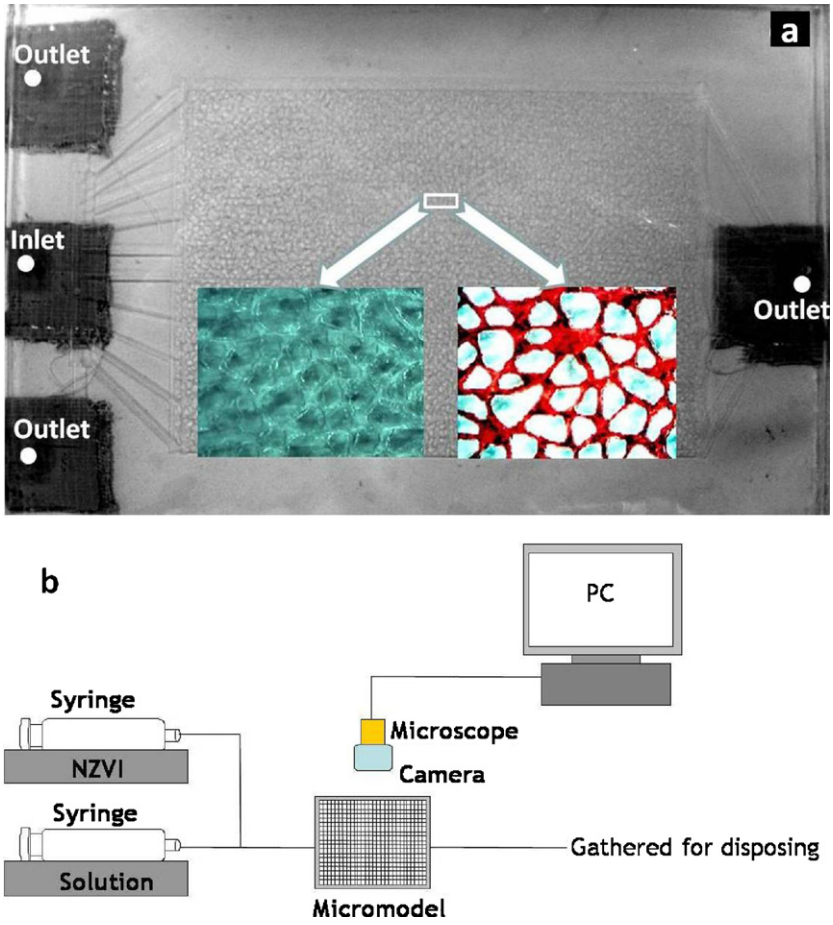

Fig. 1. Micromodel pattern (a) and schematic of the experimental setup (b).

for the simultaneous injection of two different fluids. A T-shaped tube connector (Upchurch Scientific Co.) was connected by three PTFE tubes (2 mm OD × 1.5 mm ID). Two syringe pumps then delivered an aqueous NZVI solution (0.5 g/L, 20 mL, 20 mL/h) and target solution (pH 7.0 ± 0.1); at the T-shaped connector, the separate fluids met and were subsequently injected into the inlet of the micromodel.

2.5. Residual TCE preparation, NZVI injection, and calculation of TCE DNAPL removal

The TCE was dyed with 0.1% oil-red-o in order to distinguish it from the background, thereby permitting the quantification of its saturation in the micromodel through an image analysis technique. The micromodel was sequentially cleaned once by 0.05 M sulfuric acid and ethanol, following each experiment. Before injecting the TCE DNAPL, the micromodel was flushed with the background solution to remove background turbidity and to provide a uniform collector surface charge.

Dyed TCE was injected into the micromodel which had been saturated with SGW until breakthrough at the outlet was reached. The amount of TCE DNAPL injected was around 5% of the total pore volume (PV) of the micromodel, and the TCE blobs were trapped at the inner surfaces of pores in the micromodel. The micromodel was also flushed with background solution for 40 PV in order to confirm the immobility of trapped TCE blobs, not able to be washed by DI water/background solution, in micromodel.

After the micromodel was placed with non-movable TCE blobs, NZVI or bimetallic nanoparticles with background solution were then injected into the micromodel. The injected nanoparticles

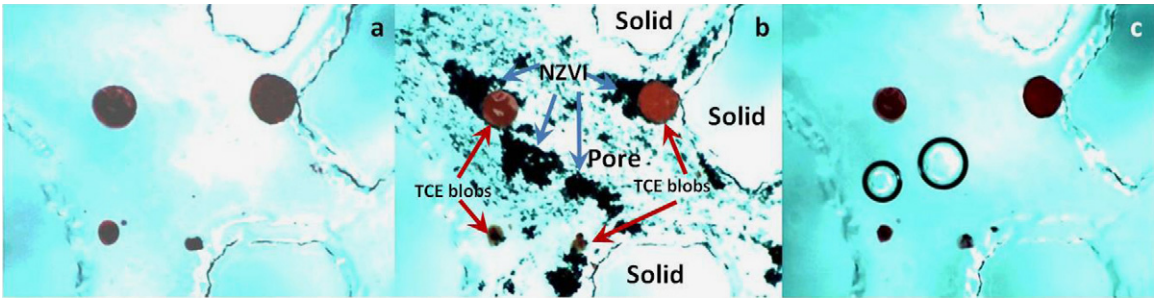

Fig. 2. Process of TCE blobs removal using NZVI in micromodel: 'a' is the initial condition, TCE blobs trapped in the pores of micromodel; 'b' is TCE blobs coated by NZVI particles; and 'c' is the final image, after 36 h TCE blobs removal by NZVI, NZVI on the surface of TCE blobs was washed by a sulfuric acid solution.

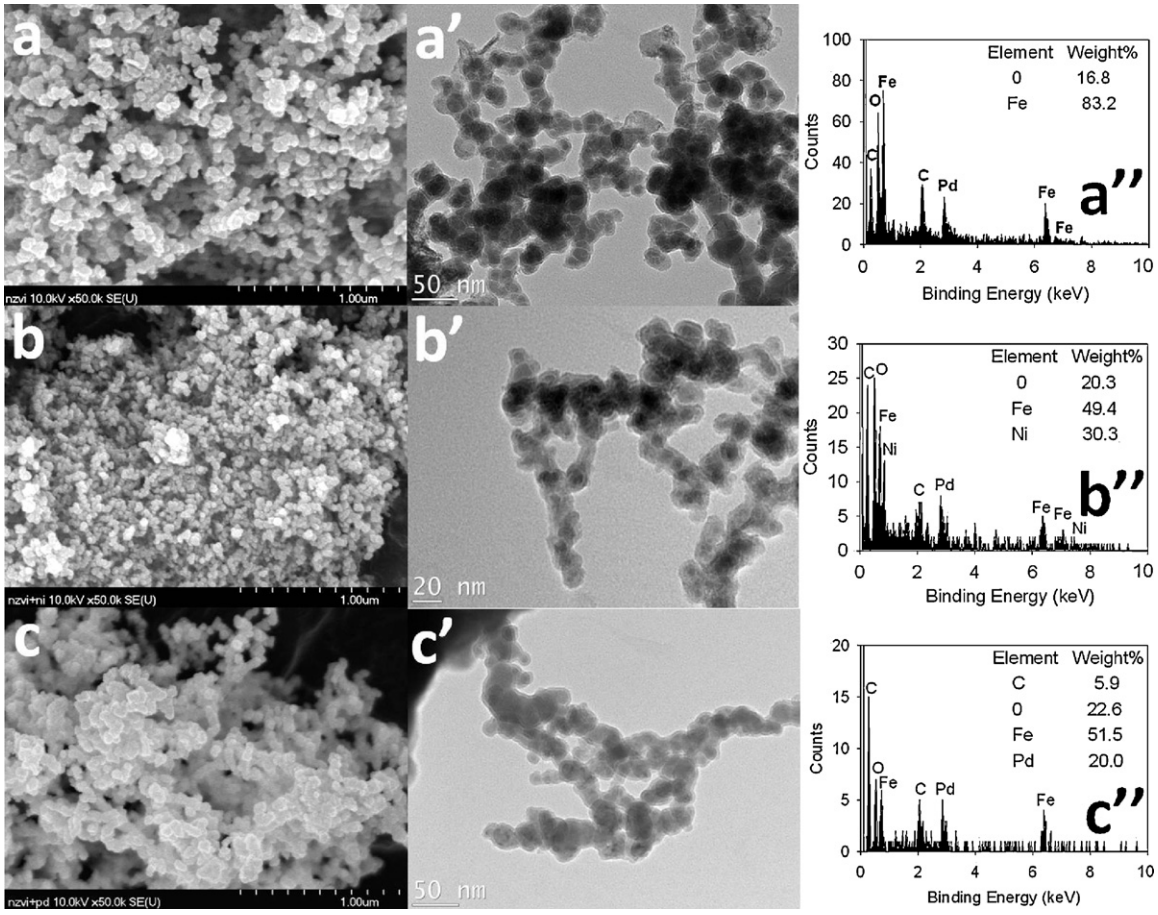

Fig. 3. SEM, TEM and EDX results of synthesized: 'a' NZVI, 'b' NZVI/Ni, and 'c' NZVI/Pd.

(0.5 g/L) were continuously sonicated using a sonicator (VCX-500 Vibracell, Sonics and Materials, Inc.) during injection of 5 PV particle solutions.

The particle solution flow was stopped after 5 PV of flow, and then 36 h were allowed for reaction between TCE blobs and the metallic nanoparticles: in the long term evaluation of NZVI, NZVI/Ni, and NZVI/Pd, 504 h (21 days) was allowed for reaction. After reaction, the deposited metallic nanoparticles coating the TCE blobs surfaces were then washed using a 30% sulfuric acid solution (see Fig. 2). The TCE DNAPL removal was quantified by calculating the difference in the TCE blobs area between the TCE blobs trapped in the micromodel prior to nanoparticles injection and the TCE blobs trapped in the micromodel after reaction [22–24]. It is well known that dissolution of NAPL into the aqueous phase results in shrinkage of NAPL blobs [28,29]. The volume of TCE blobs placed in the micromodel can be obtained by directly measuring the area of TCE blobs, because the micromodel system is a 2-dimensional system having a uniform thickness. Therefore, the TCE blobs area (i.e., the TCE blob volume) was calculated as an average of measurement of 40–50 TCE blobs trapped in the micromodel using a microscope with digital camera.

3. Results and discussion

3.1. Characterizations of synthesized NZVI and bimetallic nanoparticles

The XRD analyses of manufactured nanoparticles are shown in Fig. S1 (Supplementary material). The predominant features of the nanoparticles consist primarily of iron metal, iron corrosion, nickel, and palladium in various forms. The quantities of iron, nickel, and

Table 2
Element component % in NZVI and bimetals determined by ICP-OES.

Sample name	Total Fe content (wt%)	B content (wt%)	Na content (wt%)	Ni content (wt%)	Pd content (wt%)
NZVI	91.5	4.16	4.12	–	–
NZVI/Ni	69.4	6.35	6.63	19.6	–
NZVI/Pd	84.2	4.76	7.74	–	3.10

Table 3
Surface atomic percentage (%) for NZVI and bimetals determined by XPS.

Samples	Fe	O	C	Na	B	Ni	Pd
NZVI	13.21	52.69	19.10	4.97	10.04	–	–
Bimetallic (Fe/Ni)	8.14/4.31	54.97	32.59	1.05	3.02	4.31	–
Bimetallic (Fe/Pd)	13.24/0.75	50.23	35.77	2.21	–	–	0.75

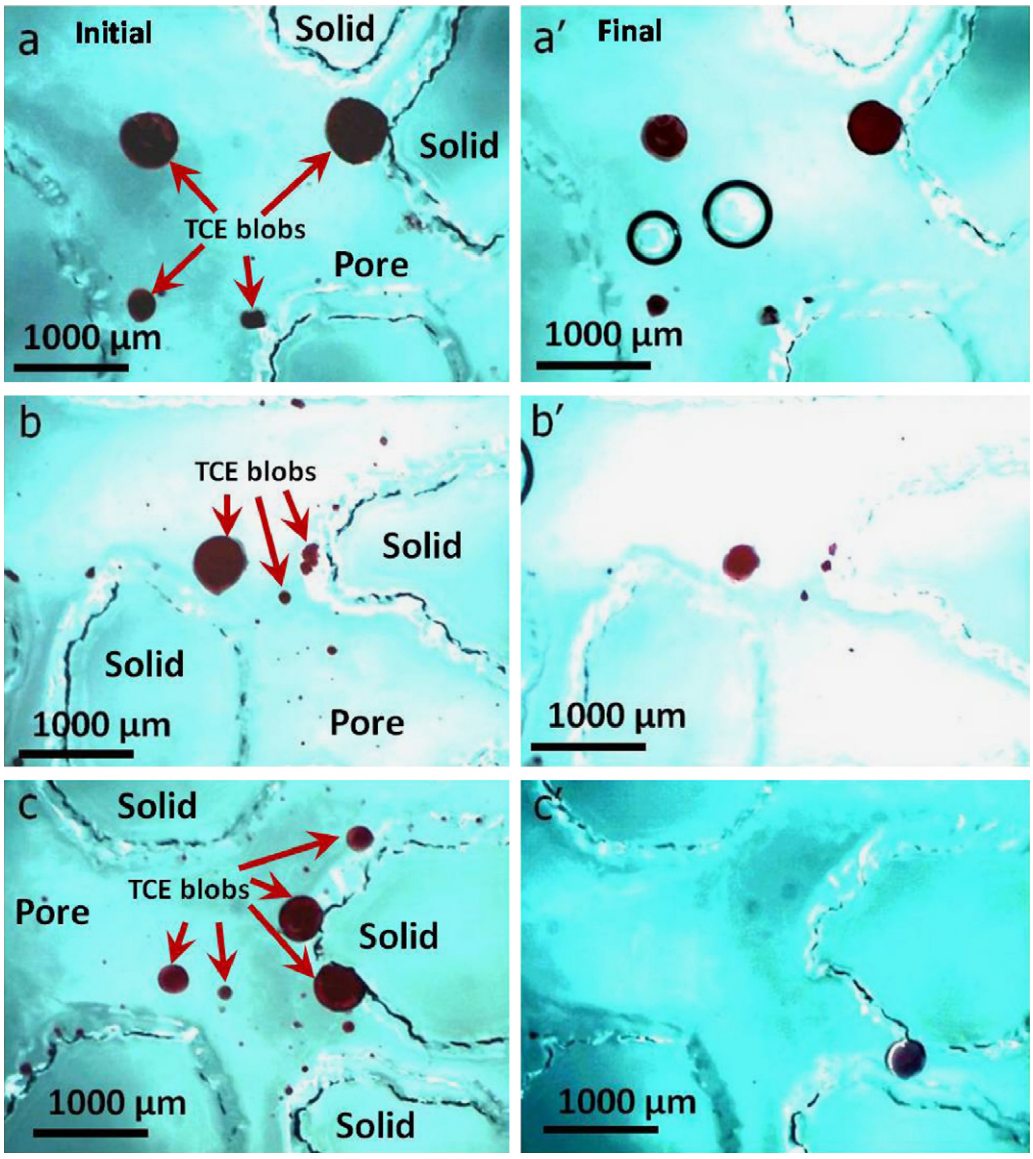

Fig. 4. Images from the porous pattern glass model where the residual TCE DNAPL was removed by NZVI in the presence of co-solvent (red blob is TCE): 'a' in DI water solution, 'b' in 20% ethanol aqueous solution, and 'c' in 50% ethanol aqueous solution. (For interpretation of the references to color in this figure legend, the reader is referred to the web version of the article.)

palladium were also determined using ICP-OES after the nanoparticles were digested in HCl (see Table 2).

SEM, TEM, and EDX results of synthesized NZVI, NZVI/Ni, and NZVI/Pd are presented in Fig. 3a–c. The chemical compositions of the particles were determined via an EDX spectral analysis (Fig. 3a″, b″, and c″), significant Fe, O, Ni, and Pd peaks were detected; however, the carbon and the partial palladium signals are from the supporting and coating material in SEM preparation.

Fig. S2 presents the XPS wide-scan results of freshly prepared NZVI, NZVI/Ni, and NZVI/Pd. The photoelectron peaks in Fig. S2a reveal that the nanoparticle surface consists mainly of iron and oxygen, in addition to small amounts of sodium, boron, and carbon. Carbon on the NZVI surface likely originates from the inadvertent exposure to carbon dioxide and potentially small hydrocarbon molecules in air, water, and on the glassware during the sample preparation and delivery [30]. Sodium and boron at the surface are from the reagent sodium borohydride, though sodium and boron are soluble and can be rinsed off with water [31]. The photoelectron peaks in Fig. S2b and S2c reveal that nanoparticle surface also consists of nickel and palladium, which are from the synthesized bimetallic nanoparticles. Based on the individual XPS survey of elements at the surface and atomic sensitivity factors, surface compositions of NZVI and bimetallic (Fe/Ni, Fe/Pd) nanoparticles are summarized in Table 3. In addition, a detailed XPS survey for Fe 2p of NZVI and bimetallic nanoparticles regions are shown in Fig. S3, Fig. S4 shows the Ni 2p XPS spectra of the NZVI/Ni nanoparticles, the peaks at 846.6 and 852.2 eV are assigned to the features of Ni^0; and Fig. S5 shows the Pd 3d XPS spectra of the NZVI/Pd nanoparticles, the positions and the peaks with binding energies of 335.5 and 340.5 eV match the $3d_{5/2}$ and $3d_{3/2}$ peaks for Pd(0); similar results of NZVI and bimetallic nanoparticles were reported in previous researches [16,32].

3.2. TCE DNAPL removal processes by NZVI in porous media

Fig. 2 shows that TCE blob area becomes smaller as time elapses. The TCE blobs started to dissolve into the aqueous phase, and then these dissolved TCE reacted with NZVI; dissolved TCE can be efficiently degraded using NZVI. As dissolved TCE was reacted and then degraded by NZVI, TCE dissolution from TCE blobs would be

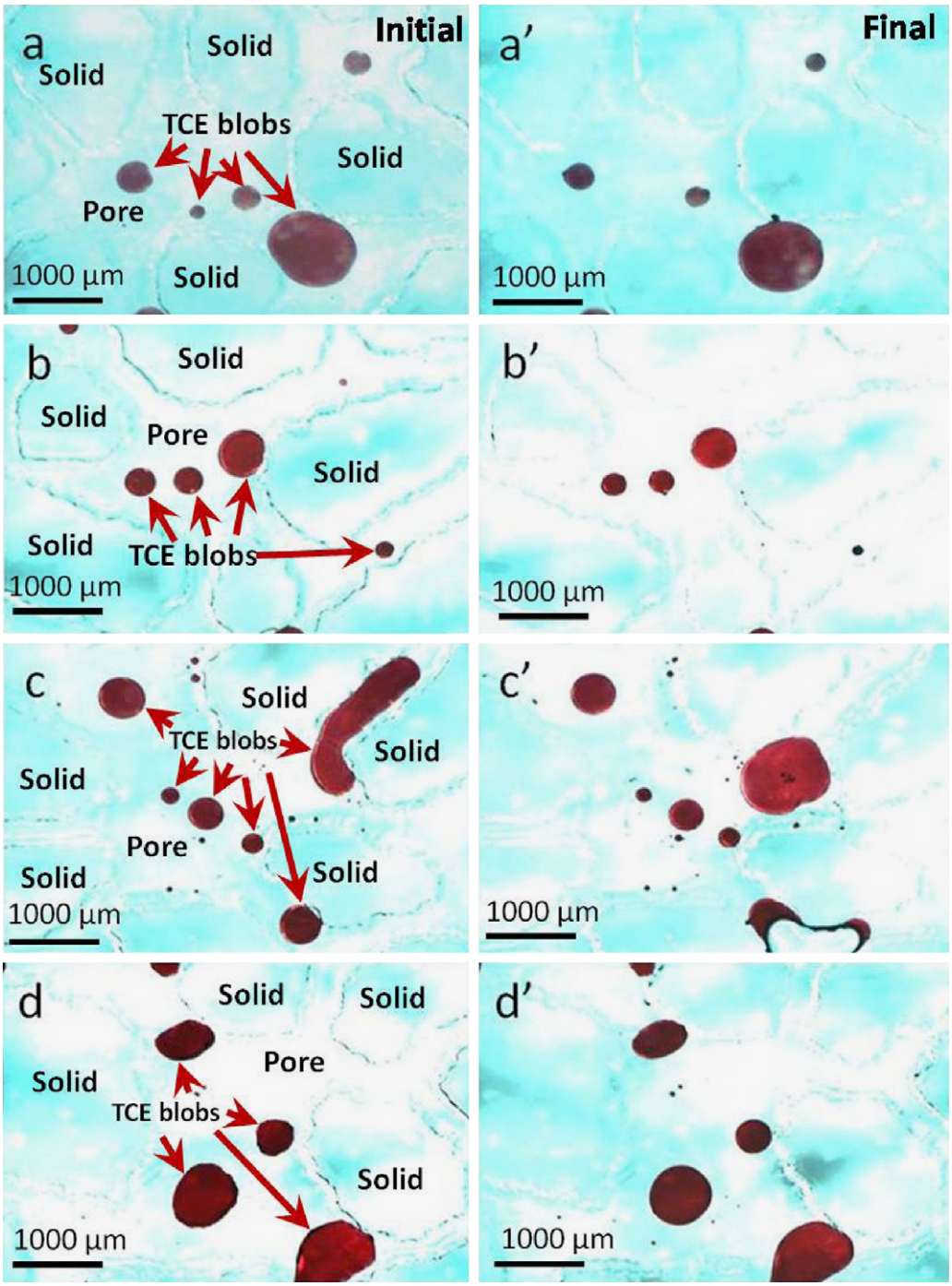

Fig. 5. Images from the porous pattern glass model where the residual TCE DNAPL was removed by NZVI in the presence of sodium nitrate (red blob is TCE). Nitrate concentrations are: (a) 4 mM, (b) 10 mM, (c) 20 mM, and (d) 40 mM.

facilitated and the TCE blob areas would be eventually reduced. Fig. S6 shows a schematic diagram explaining these mechanisms. The fate and degradation of TCE using NZVI have been systematically well described already [3].

The effect of co-solvent on the TCE removal using NZVI was then investigated using aqueous ethanol solutions of 0% (DI water), 20%, and 50% as the co-solvent. Visualizations of the TCE removal are shown in Fig. 4, where it is clearly observed that the area of TCE blobs was significantly reduced in the presence of 0%, 20%, and 50% ethanol solution. The observed TCE blobs were probably reduced by three processes: enhanced dissolution of TCE blob in aqueous ethanol solution due to the higher solubility of TCE in ethanol solution than in DI water [33], removal of dissolved TCE by NZVI, mobilization-reduction of TCE blobs. Fig. 4c and c′ show TCE blob removal using a 50% ethanol solution with NZVI. Three sequential processes, TCE blob dissolution, TCE removal by NZVI and mobilization, were observed; most of the TCE blobs were removed and the remaining blobs were shifted from their previous position. This mobilization can be attributed to the reduction in interfacial tension by increasing the ethanol concentration in the co-solvent; note that TCE mobilization was not observed in the presence of water alone (Fig. 4a, a′).

This study evaluated the reduction in TCE blob size by flooding with DI water and ethanol solution alone. Fig. 9a compares the TCE

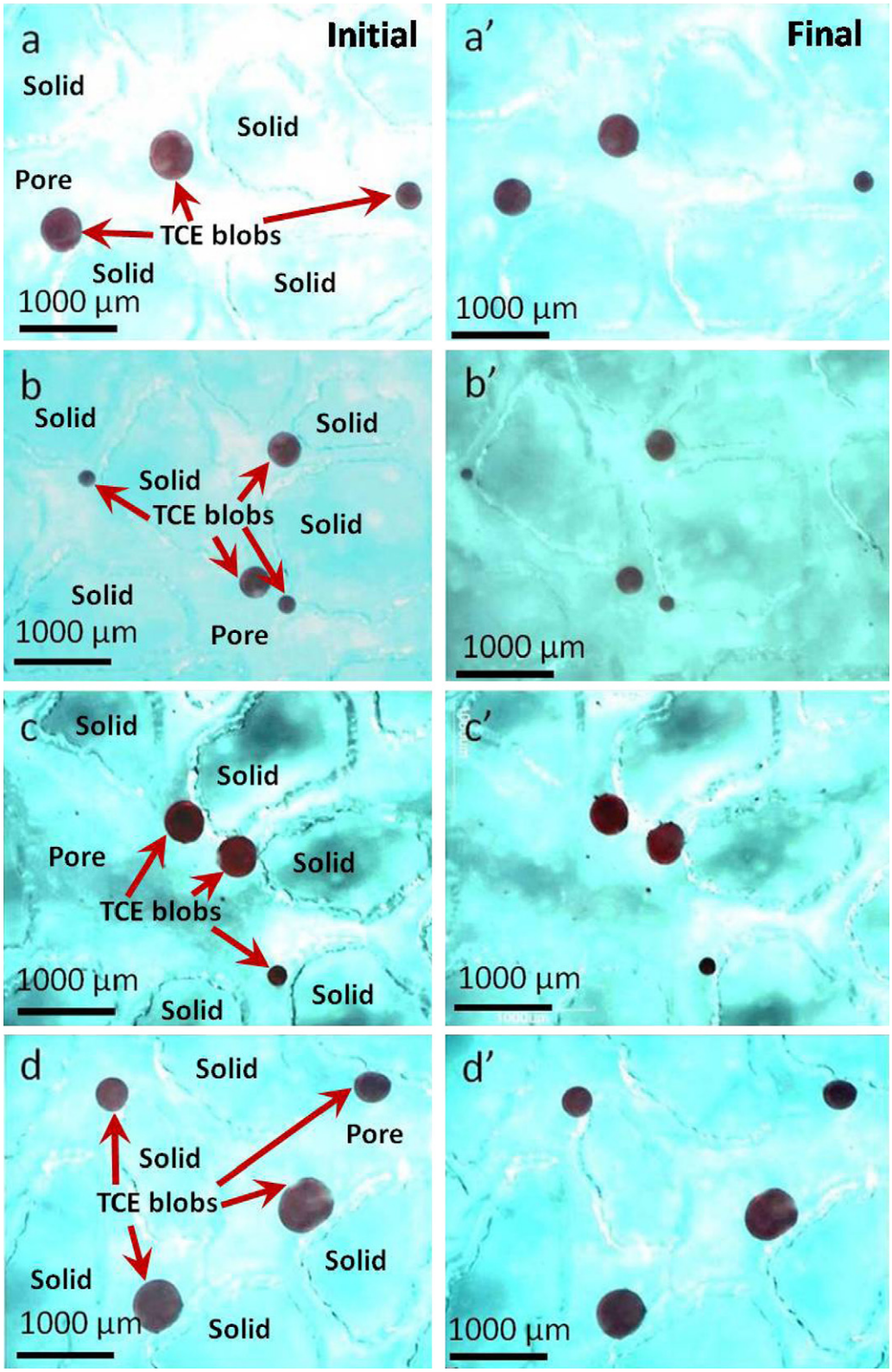

Fig. 6. Images from the porous pattern glass model where the residual TCE DNAPL was removed by NZVI in the presence of PPFA in SGW (red blob is TCE). PPFA concentrations are: (a) 0 ppm, (b) 5 ppm, (c) 10 ppm, and (d) 15 ppm.

DNAPL removal efficiencies by between NZVI with cosolvent and cosolvent alone. Note that the TCE removal efficiency was calculated by analyzing the area variation of 40–50 TCE blobs present in the micromodel. The TCE DNAPL removal only by aqueous ethanol washing was less than the TCE DNAPL removal by NZVI under an aqueous ethanol condition. These results implied that reduction of dissolved TCE by NZVI accelerated dissolution of TCE blob and eventually resulted in reduction in TCE blob size.

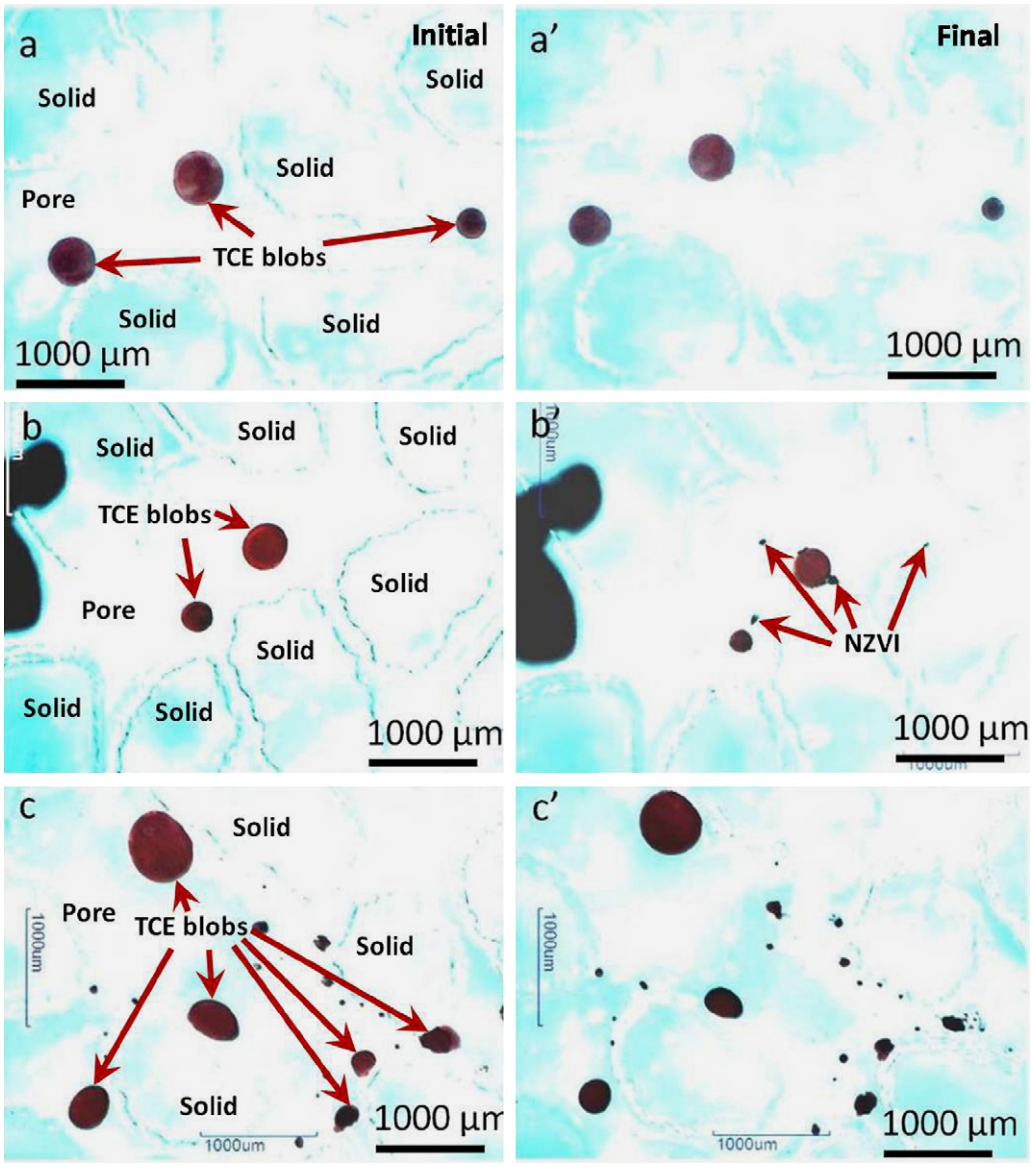

Fig. 7. Images from the porous pattern glass model where the residual TCE DNAPL was removed by NZVI and bimetallic nanoparticles during a short-term reaction in SGW: (a) NZVI, (b) NZVI/Ni, and (c) NZVI/Pd.

3.3. Effect of nitrate on TCE DNAPL removal by NZVI

The TCE DNAPL removal by NZVI was inhibited in the presence of nitrate at concentrations of 4–40 mM. Visualization of the TCE DNAPL removal is shown in Fig. 5 and those removal efficiencies were in the order of 4 mM > 10 mM > 20 mM > 40 mM (see Fig. 9b). One possible explanation for this inhibition in the existence of NO_3^- is competition between NO_3^- and TCE for reactive sites on NZVI [34]. Additionally, upon further consideration, another evident explanation is that the hindrance is resulted from surface passivation at higher NO_3^- concentrations, which results in iron oxide/hydroxide (FeOOH) forming on the NZVI surface. This FeOOH forming changes the TCE removal reaction from cathodic control (i.e., reduction of TCE) to anodic control (i.e., release of Fe^{2+} and electrons) [35]. Schlicker et al. [36] also reported that the nitrate removal rate by NZVI is faster than TCE removal rate. In the micromodel, NZVI would prefer to react with nitrate rather than the dissolved TCE. Although the nitrate inhibition by the previous studies was observed with the dissolved TCE, this study also found the nitrate inhibition effect on removal of TCE DNAPL by NZVI.

3.4. Effect of humic substance on TCE DNAPL removal by NZVI

The visualizations of TCE removal in the presence of PPFA are shown in Fig. 6. Conditions of the PPFA concentration in Fig. 6 were 0, 5, 10, 15 ppm, from Fig. 6a to d. Fig. 6 shows the initial images and the final images after reaction. The image analyzer showed that the TCE blob size in these images of Fig. 6 was reduced by at least 10% from the initial size, although it was hard to find the difference with the naked eye. Fig. 9c shows the overall quantification results of TCE DNAPL removal efficiency. The overall TCE DNPL removal efficiency obtained by analysis of tens of TCE blobs showed they are apparently different from each other.

As concentrations of PPFA increase, the TCE removal efficiencies decreased (see Fig. 9c); additionally, decrease of the TCE blob area in the presence of PPFA is in the order of 0 ppm > 5 ppm > 10 ppm > 15 ppm. PPFA is known to readily adsorb to iron (hydr) oxides [37], and many (hydr) oxide phases are typically present on the surface of NZVI. Hence, PPFA adsorption onto iron surfaces is depicted by nonspecific surface interactions: free energy changes associated with PPFA solvation, electrostatic

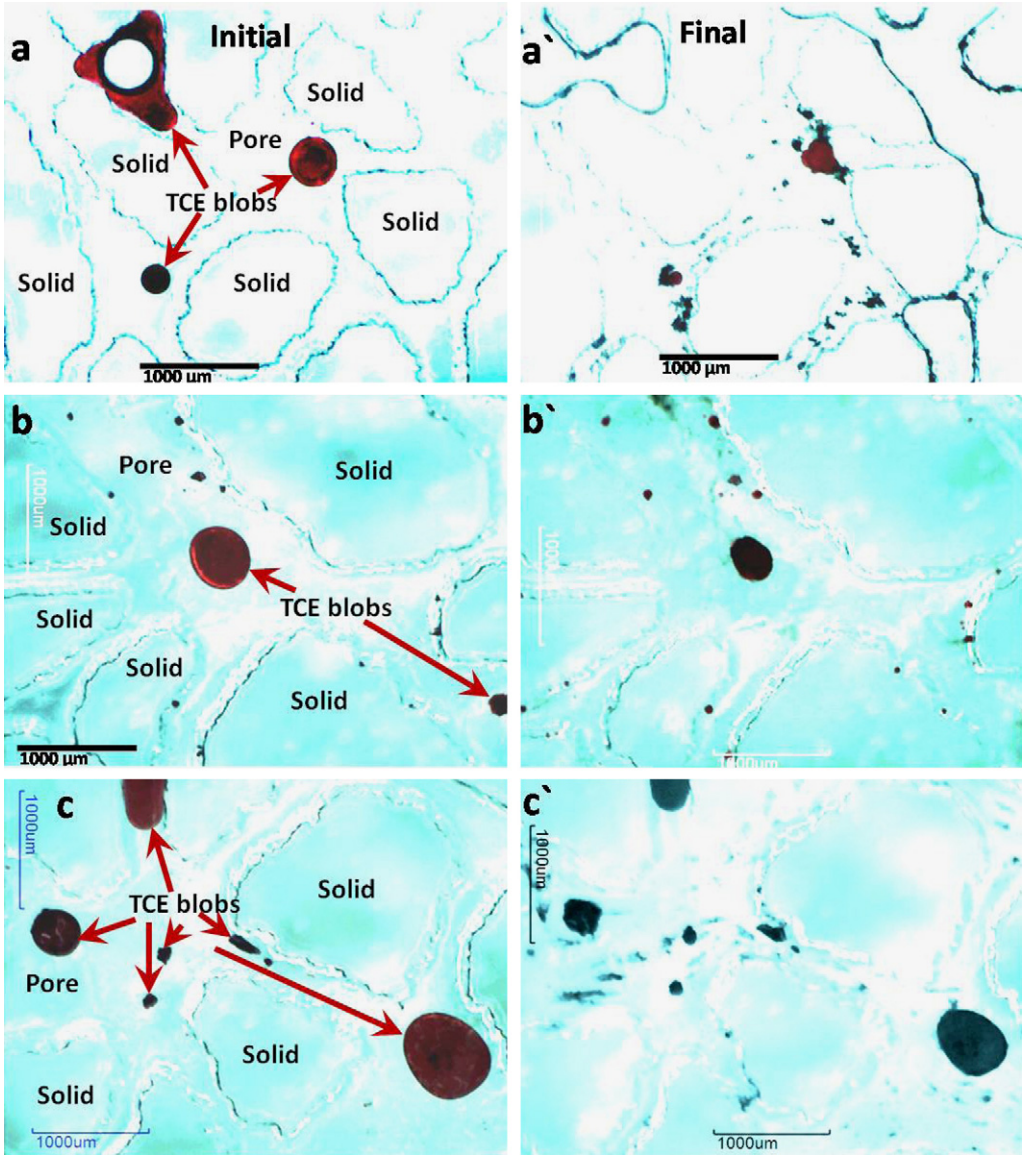

Fig. 8. Images from the porous pattern glass model where the residual TCE DNAPL was removed by NZVI and bimetallic nanoparticles during a long-term (504 h) reaction in SGW: (a) NZVI, (b) NZVI/Ni, and (c) NZVI/Pd.

interactions between the oxide surface and the PPFA molecule, and the specific interactions that occur between functional groups in PPFA molecules and oxide surfaces [37]. As a result of the stronger PPFA–iron interactions, species such as TCE that are expected to form weakly bonded surface complexes [38] may be competitively excluded from the surface. In addition to this predominantly steric effect, adsorption of PPFA to the particle surface is expected to alter the reduction potential of neighboring Fe (II) surface sites, making them poorer reductants. Although the humic substance inhibition by the previous studies was observed with the dissolved TCE, this study further verified the previous study results with visualization and quantification of TCE DNAPL reduction.

3.5. *Effect of catalyst metal loading (bimetal) on TCE DNAPL removal*

NZVI particles containing nickel and palladium were observed to exhibit drastically different reactivity for TCE removal (Fig. 7). In image analysis of Fig. 7b and c, NZVI (Ni) reduced the TCE blob size by 35% from the initial size, while NZVI (Pd) showed 30%. Difference in the TCE blob size was apparently found in the TCE DNAPL removal efficiency results as shown in Fig. 9d. As shown in Fig. 9d, enhanced TCE DNAPL removal rates were found in application of bimetallic nanoparticles (i.e., in the order of NZVI/Ni > NZVI/Pd > NZVI). The reactivity of NZVI/Ni (with 20% Ni) and NZVI/Pd (with 5% Pd) were increased 65.8% and 36.4% comparing to pristine NZVI. The measured nickel and palladium contents were the mass ratio of nickel and palladium to iron based on the assumption that the employed nickel and palladium were completely reduced and deposited onto the iron surface:

$$Ni^{2+} + Fe \rightarrow Ni + Fe^{2+} \quad (1)$$

$$Pd^{2+} + Fe \rightarrow Pd + Fe^{2+} \quad (2)$$

Plausible explanations for this improved TCE DNAPL removal phenomenon have been proposed by the formation of a galvanic cell [39] and the surface coverage of catalytic metal on the reductive metal [40]. In addition, adsorbed atomic hydrogen can improve the dechlorination of chlorinated hydrocarbons in bimetallic systems

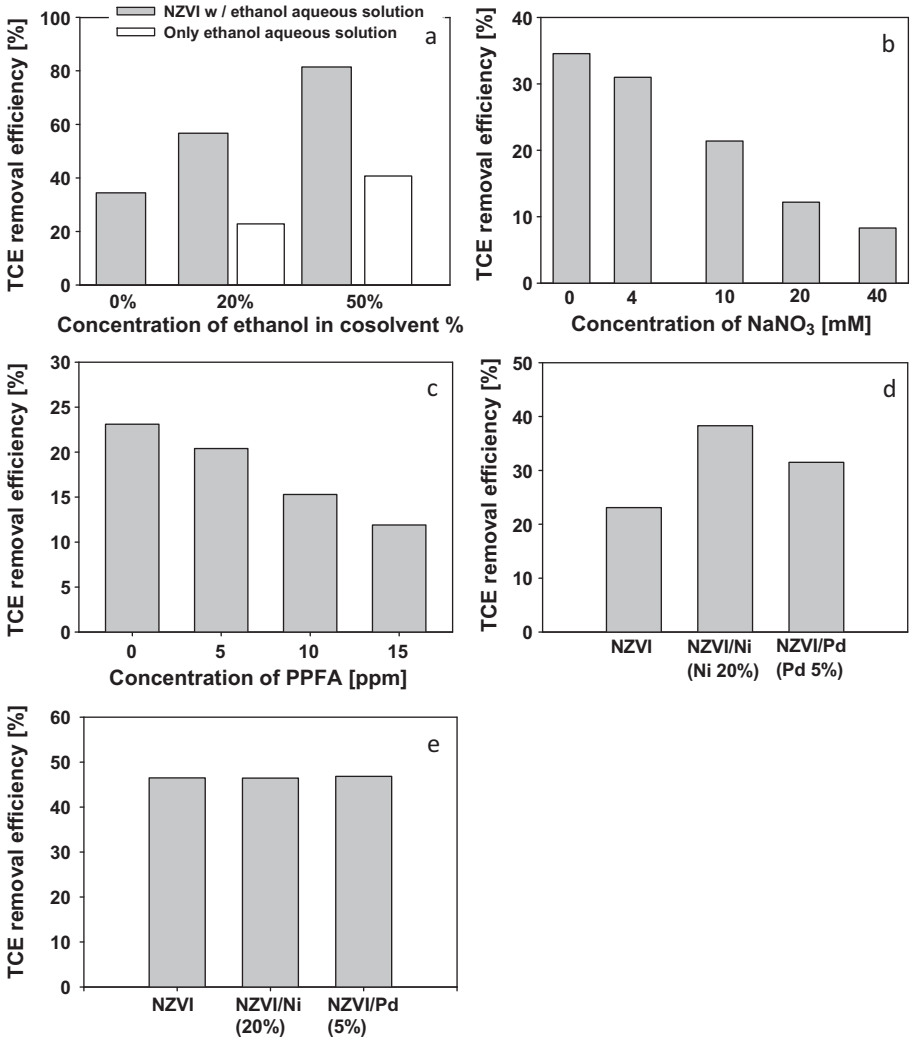

Fig. 9. TCE DNAPL removal efficiencies under different conditions: 'a' is the effect of co-solvent, 'b' is the effect of presence of nitrate, 'c' is the effect of presence of PPFA, 'd' is the effect of catalyst metal loading in short-term reaction, and 'e' is the effect of catalyst metal loading in long-term reaction.

[41,42]. Briefly, in bimetallic system, atomic hydrogen formed more readily on catalyst metal surfaces having a low cathodic hydrogen over potential than on the metals with high hydrogen over potentials, such as iron [43]. The dissolution of water by NZVI leads to a hydrogen evolution [44] and is followed by the formation of atomic hydrogen on the catalyst metal surface. The atomic hydrogen then starts to degrade TCE through a surface-mediated process [16].

3.6. Long-term removal of TCE DNAPL using NZVI and bimetallic nanoparticles

Visualizations of long-term TCE DNAPL removal using NZVI and bimetallic nanoparticles are shown in Fig. 8. All TCE blobs shown in the initial images were significantly reduced after long-term reaction. Reduction in TCE blob size with the long-term reaction can be easily found unlike those of the short-term reaction. This study measured areas of representative TCE blobs that were chosen from tens of TCE blobs present in the micromodel. As already mentioned before, TCE removal efficiency was determined from a ratio of the final TCE blob area to the initial TCE blob area.

Long-term reaction apparently increased the TCE DNAPL removal efficiency when compared with short-term reaction results. Fig. 9e shows that TCE DNAPL removal efficiencies were increased to 46% using pristine NZVI, NZVI/Ni, and NZVI/Pd bimetallic nanoparticles in SGW after 504 h. This result demonstrates the TCE DNAPL removal will reach equivalent after long-term reaction among NZVI and bimetallic nanoparticles. This phenomenon can be explained by the fact that Ni and Pd as catalysts are able to increase the rate of TCE DNAPL removal by NZVI through providing lower activation energy than NZVI alone; however, they cannot change the extent of the reaction and have no effect on the chemical equilibrium of the reaction [45]. Therefore, this study found from visualization and quantification of TCE blobs that the extent of TCE removal using NZVI and/or bimetallic nanoparticles will be equal when the TCE DNAPL removal by NZVI was allowed with enough time to complete this reaction.

TCE blobs existed for a long time even though all TCE blobs were fully exposed to iron and bimetallic nanoparticles. Micromodel visualization results imply that DNAPL placed in source areas where iron and bimetallic nanoparticles were applied for remediation exist for a relatively long time. DNAPL would persist longer if there are relatively high humic substance and nitrate present in groundwater. DNAPL can continuously release dissolved TCE component unless it disappears in the subsurface. Enhanced dissolution of DNAPL would be primarily tried for remediating source areas by iron and bimetallic nanoparticles.

4. Conclusions

This study demonstrated a novel approach for first revealing the TCE DNAPL removal inside pore areas using iron and bimetallic nanoparticles in porous media through visualization technique. Representative TCE blobs were selected and continuously monitored for quantifying those areas. TCE DNAPL removal was determined as the difference of DNAPL blobs area between the initial DNAPL blobs area and the area remaining after reaction.

The TCE DNAPL removal efficiency was found to decrease when nitrate and humic substance were present in the solution; however, the presence of ethanol in the solution increased the TCE DNAPL removal efficiency. Three sequential TCE DNAPL removal mechanisms by NZVI were suggested by visualization and quantification results: as dissolved TCE was reacted and then degraded by NZVI, TCE dissolution from TCE blobs would be facilitated and the TCE blob areas would be eventually reduced. The presence of catalysts (Ni and Pd in bimetallic nanoparticles) enhanced the TCE DNAPL removal in short-term reaction (36 h); however, over long-term reaction (21 days), the presence of catalysts did not change the extent of TCE DNAPL removal. Catalysts emplaced in NZVI would not affect the overall TCE DNAPL removal in the pores but the destruction rate of TCE DNAPL in the beginning of reaction. Direct TCE DNAPL observation clearly showed that TCE blobs existed in pores for a long time even though TCE blobs were fully exposed to iron and bimetallic nanoparticles. This study implies that the successful application of a NZVI-based remediation technology for DNAPL source areas may require significant enhancement in DNAPL dissolution.

Acknowledgment

This work was supported by the National Research Foundation grant funded by the Korea Government (R01-2007-000-21106-0).

Appendix A. Supplementary data

Supplementary data associated with this article can be found, in the online version, at doi:10.1016/j.jhazmat.2012.02.002.

References

[1] P.T. Imhoff, S.N. Gleyzer, J.F. McBride, L.A. Vancho, I. Okuda, C.T. Miller, Cosolvent-enhanced remediation of residual dense nonaqueous phase liquids: experimental investigation, Environ. Sci. Technol. 29 (1995) 1966–1976.
[2] H.-S. Kim, J.-Y. Ahn, K.-Y. Hwang, I.-K. Kim, I. Hwang, Atmospherically stable nanoscale zero-valent iron particles formed under controlled air contact: characteristics and reactivity, Environ. Sci. Technol. 44 (2010) 1760–1766.
[3] Y. Liu, S.A. Majetich, R.D. Tilton, D.S. Sholl, G.V. Lowry, TCE dechlorination rates, pathways, and efficiency of nanoscale iron particles with different properties, Environ. Sci. Technol. 39 (2005) 1338–1345.
[4] S.W. Jeong, A.L. Wood, T.R. Lee, Enhanced removal of DNAPL trapped in porous media using simultaneous injection of cosolvent with air: influencing factors and removal mechanisms, J. Hazard. Mater. 101 (2003) 109–122.
[5] P.T. Imhoff, C.T. Miller, Dissolution fingering during the solubilization of nonaqueous phase liquids in saturated porous media 1. Model predictions, Water Resour. Res. 32 (1996) 1919–1928.
[6] Y. Yang, P.L. McCarty, Biologically enhanced dissolution of tetrachloroethene DNAPL, Environ. Sci. Technol. 34 (2000) 2979–2984.
[7] L. Yan, K.E. Thompson, K.T. Valsaraj, D.D. Reible, In situ control of DNAPL density using polyaphrons, Environ. Sci. Technol. 37 (2003) 4487–4493.
[8] E.H. Hill, M. Moutier, J. Alfaro, C.T. Miller, Remediation of DNAPL pools using dense brine barrier strategies, Environ. Sci. Technol. 35 (2001) 3031–3039.
[9] C.T. Miller, E.H. Hill, M. Moutier, Remediation of DNAPL-contaminated subsurface systems using density-motivated mobilization, Environ. Sci. Technol. 34 (2000) 719–724.
[10] W.S. Orth, R.W. Gillham, Dechlorination of trichloroethene in aqueous solution using Fe^0, Environ. Sci. Technol. 30 (1995) 66–71.
[11] I. Okuda, J.F. McBride, S.N. Gleyzer, C.T. Miller, Physicochemical transport processes affecting the removal of residual DNAPL by nonionic surfactant solutions, Environ. Sci. Technol. 30 (1996) 1852–1860.
[12] S.-W. Jeong, M.Y. Corapcioglu, S.E. Roosevelt, Micromodel study of surfactant foam remediation of residual trichloroethylene, Environ. Sci. Technol. 34 (2000) 3456–3461.
[13] T.C.G. Kibbey, C.A. Ramsburg, K.D. Pennell, K.F. Hayes, Implications of alcohol partitioning behavior for in situ density modification of entrapped dense nonaqueous phase liquids, Environ. Sci. Technol. 36 (2002) 104–111.
[14] G.A. Loraine, Effects of alcohols, anionic and nonionic surfactants on the reduction of pce and tce by zero-valent iron, Water Res. 35 (2001) 1453–1460.
[15] N. Saleh, T. Phenrat, K. Sirk, B. Dufour, J. Ok, T. Sarbu, K. Matyjaszewski, R.D. Tilton, G.V. Lowry, Adsorbed triblock copolymers deliver reactive iron nanoparticles to the oil/water interface, Nano Lett. 5 (2005) 2489–2494.
[16] H.-L. Lien, W.-X. Zhang, Nanoscale Pd/Fe bimetallic particles: catalytic effects of palladium on hydrodechlorination, Appl. Catal. B-Environ. 77 (2007) 110–116.
[17] Q. Wang, S. Snyder, J. Kim, H. Choi, Aqueous ethanol modified nanoscale zerovalent iron in bromate reduction: synthesis, characterization, and reactivity, Environ. Sci. Technol. 43 (2009) 3292–3299.
[18] G.V. Lowry, M. Reinhard, Pd-catalyzed TCE dechlorination in groundwater: solute effects, biological Control, and oxidative catalyst regeneration, Environ. Sci. Technol. 34 (2000) 3217–3223.
[19] N.D. Berge, C.A. Ramsburg, Iron-mediated trichloroethene reduction within nonaqueous phase liquid, J. Contam. Hydrol. 118 (2010) 105–116.
[20] A. Taghavy, J. Costanza, K.D. Pennell, L.M. Abriola, Effectiveness of nanoscale zero-valent iron for treatment of a PCE-DNAPL source zone, J. Contam. Hydrol. 118 (2010) 128–142.
[21] T. Phenrat, F. Fagerlund, T. Illangasekare, G.V. Lowry, R.D. Tilton, Polymer-modified Fe^0 nanoparticles target entrapped NAPL in two dimensional porous media: effect of particle concentration, NAPL saturation, and injection strategy, Environ. Sci. Technol. 45 (2011) 6102–6109.
[22] S.W. Jeong, M.Y. Corapcioglu, S.E. Roosevelt, Micromodel study of surfactant foam remediation of residual trichloroethylene, Environ. Sci. Technol. 34 (2000) 3456–3461.
[23] S.W. Jeong, A.L. Wood, T.R. Lee, Enhanced contact of cosolvent and DNAPL in porous media by concurrent injection of cosolvent and air, Environ. Sci. Technol. 36 (2002) 5238–5244.
[24] S.-W. Jeong, B.-K. Ju, B.-J. Lee, Effects of alcohol-partitioning type and airflow on cosolvent flooding to benzene-LNAPL saturated porous media, J. Hazard. Mater. 166 (2009) 603–611.
[25] Q. Wang, J.-H. Lee, S.-W. Jeong, A. Jang, S. Lee, H. Choi, Mobilization and deposition of iron nano and sub-micrometer particles in porous media: a glass micromodel study, J. Hazard. Mater. 192 (2011) 1466–1475.
[26] J. Dries, L. Bastiaens, D. Springael, S.N. Agathos, L. Diels, Competition for sorption and degradation of chlorinated ethenes in batch zero-valent iron systems, Environ. Sci. Technol. 38 (2004) 2879–2884.
[27] Q. Wang, S. Lee, H. Choi, Aging study on the structure of Fe^0-nanoparticles: stabilization, characterization, and reactivity, J. Phys. Chem. C 114 (2010) 2027–2033.
[28] S.E. Powers, L.M. Abriola, W.J. Weber Jr., An experimental investigation of nonaqueous phase liquid dissolution in saturated subsurface systems: transient mass transfer rates, Water Resour. Res. 30 (1994) 321–332.
[29] N.A. Sahloul, M.A. Ioannidis, I. Chatzis, Dissolution of residual non-aqueous phase liquids in porous media: pore-scale mechanisms and mass transfer rates, Adv. Water Res. 25 (2002) 33–49.
[30] X.-Q. Li, W.-X. Zhang, Sequestration of metal cations with zerovalent iron nanoparticles: a study with high resolution X-ray photoelectron spectroscopy (HR-XPS), J. Phys. Chem. C 111 (2007) 6939–6946.
[31] J.T. Nurmi, P.G. Tratnyek, V. Sarathy, D.R. Baer, J.E. Amonette, K. Pecher, C. Wang, J.C. Linehan, D.W. Matson, R.L. Penn, M.D. Driessen, Characterization and properties of metallic iron nanoparticles: spectroscopy, electrochemistry, and kinetics, Environ. Sci. Technol. 39 (2005) 1221–1230.
[32] R. Muftikian, K. Nebesny, Q. Fernando, N. Korte, X-ray photoelectron spectra of the palladium–iron bimetallic surface used for the rapid dechlorination of chlorinated organic environmental contaminants, Environ. Sci. Technol. 30 (1996) 3593–3596.
[33] R.C. Chawla, K.F. Doura, D. McKay, Effect of alcohol cosolvents on the aqueous solubility of trichloroethylene, in: Proceedings of the 2001 Conference on Environmental Research, 2001, pp. 52–66.
[34] Y. Liu, T. Phenrat, G.V. Lowry, Effect of TCE concentration and dissolved groundwater solutes on NUI-promoted TCE dechlorination and H-2 evolution, Environ. Sci. Technol. 41 (2007) 7881–7887.
[35] J. Farrell, M. Kason, N. Melitas, T. Li, Investigation of the long-term performance of zero-valent iron for reductive dechlorination of trichloroethylene, Environ. Sci. Technol. 34 (2000) 514–521.
[36] O. Schlicker, E. Markus, F. Margit, W. Markus, W. Wolfgang, D. Andreas, Degradation of TCE with iron: the role of competing chromate and nitrate reduction, Ground Water 38 (2000) 403–409.
[37] J.A. Davis, Adsorption of natural dissolved organic matter at the oxide/water interface, Geochim. Cosmochim. Acta 46 (1982) 2381–2393.
[38] W.A. Arnold, A.L. Roberts, Pathways and kinetics of chlorinated ethylene and chlorinated acetylene reaction with Fe(0) particles, Environ. Sci. Technol. 34 (2000) 1794–1805.
[39] Y.H. Liou, S.L. Lo, C.J. Lin, C.Y. Hu, W.H. Kuan, S.C. Weng, Methods for accelerating nitrate reduction using zerovalent iron at near-neutral pH: effects of H_2-reducing pretreatment and copper deposition, Environ. Sci. Technol. 39 (2005) 9643–9648.

[40] C.-C. Lee, R.-A. Doong, Dechlorination of tetrachloroethylene in aqueous solutions using metal-modified zerovalent silicon, Environ. Sci. Technol. 42 (2008) 4752–4757.
[41] J. Wang, J. Farrell, Investigating the role of atomic hydrogen on chloroethene reactions with iron using Tafel analysis and electrochemical impedance spectroscopy, Environ. Sci. Technol. 37 (2003) 3891–3896.
[42] I.F. Cheng, Q. Fernando, N. Korte, Electrochemical dechlorination of 4-chlorophenol to phenol, Environ. Sci. Technol. 31 (1997) 2443.
[43] J.H. Brewster, Mechanisms of reductions at metal surfaces. I. A general working hypothesis, J. Am. Chem. Soc. 76 (1954) 6361–6363.
[44] Y.Q. Liu, G.V. Lowry, Effect of particle age (Fe^0 content) and solution pH on NZVI reactivity: H_2 evolution and TCE dechlorination, Environ. Sci. Technol. 40 (2006) 6085–6090.
[45] http://en.wikipedia.org/wiki/Catalyst.